

DOI: 10.1002/adem.200900122

# Influence of Treatment Conditions on the Chemical Oxidative Activity of H<sub>2</sub>SO<sub>4</sub>/H<sub>2</sub>O<sub>2</sub> Mixtures for Modulating the Topography of Titanium\*\*

By Fabio Variola, Alessandro Lauria, Antonio Nanci\* and Federico Rosei\*

Host-tissue integration of medical implants is governed by their surface properties. The capacity to rationally design the surface physico-chemical cues of implantable materials is thus a fundamental prerequisite to confer enhanced biocompatibility. Our previous work demonstrated that different cellular processes are elicited by the nanotexture generated on titanium (cpTi) and Ti6Al4V alloy by chemical oxidation with a H<sub>2</sub>SO<sub>4</sub>/H<sub>2</sub>O<sub>2</sub> mixture. Here, we illustrate that by varying the etching parameters such as temperature, concentration, and treatment time, we can create a variety of surface features on titanium which are expected to impact its biological response. The modified submicron and nanotextured surfaces were characterized by scanning electron (SEM) and atomic force (AFM) microscopies. Contact angle measurements revealed the higher hydrophilicity of the modified surfaces compared to untreated samples and Fourier transform infrared spectroscopy (FT-IR) established that the etching generated a TiO<sub>2</sub> layer with a thickness in the 40–60 nm range.

[\*] Prof. F. Rosei, F. Variola

INRS-EMT, Université du Québec, 1650 Boul. Lionel-Boulet  
Varennes, QC, J3X 1S2, Canada

E-mail: rosei@emt.inrs.ca

Prof. A. Nanci, F. Variola, Dr. A. Lauria

Laboratory for the Study of Calcified Tissues and Biomaterials,  
Faculté de Médecine

Dentaire

Université de Montréal, Montreal, QC, H3C 3J7, Canada

E-mail: Antonio.nanci@umontreal.ca

Dr. A. Lauria

Department of Materials Science, University of Milano  
Bicocca

Milano, Italy

[\*\*] Acknowledgments: We acknowledge funding from the Canadian Institutes of Health Research (CIHR) and the Natural Sciences and Engineering Research Council of Canada (NSERC) through a Collaborative Health Research Project grant. In addition, we thank NSERC for a Collaborative Research and Development grant with Plasmionique, Inc. (Varennes, QC, Canada). F. V. acknowledges the Canadian Bureau for International Education (CBIE) and FQRNT for graduate fellowships. A. N. acknowledges funding from the CIHR and the Canada Foundation for Innovation (CFI). F. R. is grateful to the Fonds québécois de la recherche sur la nature et les technologies (FQRNT) and the CFI. F. R. also acknowledges support from the Canada Research Chairs Program for partial salary support and from NSERC (Discovery Grants).

Implantable materials are required to have particular mechanical and physico-chemical properties to assure appropriate functioning and durability of medical devices.<sup>[1,2]</sup> These characteristics may vary according to the intended application, however in all cases implantable materials must exhibit biocompatibility.<sup>[3]</sup> That is they must be tolerated by the human body to avoid allergic immune reactions which could eventually lead to implant failure.<sup>[4]</sup> However, the current trend in health-related research aims to confer to implantable materials additional biological properties such as the ability to promote tissue regeneration. The capacity to actively interact with the surrounding tissues, to promote improved biological responses and to guide cellular processes along predetermined pathways, has thus become a primary objective in the design of novel generations of biomaterials.

It is now recognized that implant-host tissue interactions are regulated by specific surface properties, such as its chemical composition, energy, roughness, and topography.<sup>[5–11]</sup> The key to achieving improved bioactivity is the rational design of a material's surface properties. Several physical and chemical methods have been adopted to modify, at different scales, the surface properties of widely used biomaterials toward an improved bioactivity.<sup>[12–14]</sup> Over the past few years, attention has focused on nanoscale surface modifications to improve biointegration, such as by creating specific nanogeometries, and on the ability to superimpose nanoscale features on microtopography (reviewed in ref. [14]).

We have recently demonstrated that a bioactive nanoporous structure can be created on commercially pure grade 2 titanium (cpTi)<sup>[15,16]</sup> and on the Ti6Al4V alloy<sup>[17,18]</sup> by simple oxidative nanopatterning with a 50% v/v mixture of concentrated sulfuric acid ( $\text{H}_2\text{SO}_4^{\text{conc}}$ ) and 30% aqueous hydrogen peroxide ( $\text{H}_2\text{O}_2^{\text{aq}}$ ). This treatment conferred to these two materials novel biological properties, such as improved osteoconductivity<sup>[19,20]</sup> and the unique capacity to elicit differential cellular activities.<sup>[17,18]</sup> In the case of the alloy, it was also shown that two levels of topography (i.e., submicrometric cavities with a superimposed nanotexture) can be generated and designed by controlling the exposure time to the chemical solution.<sup>[18]</sup> These studies illustrated that bioeffective surface features at different scales can be readily created directly on titanium-based materials by exploiting the electrochemical response of cpTi and Ti6Al4V to the etching solution. The possibility to generate bioeffective micro- and nanopatterns on these materials and to control their physico-chemical characteristics by adjusting the parameters of the treatment with the  $\text{H}_2\text{SO}_4/\text{H}_2\text{O}_2$  mixture (Piranha solution) may have a significant impact in implantology. This simple yet efficient chemical approach allows significantly enhancing the biological response of titanium-based metals by conferring a surprising differential bioactivity. Because of its simplicity, its applicability to different biocompatible metals<sup>[21]</sup> and even to devices with complex geometries (e.g., dental screws), oxidative nanopatterning can be easily adopted for large-scale industrial production. Thus, we decided to extend our previous studies by determining how temperature and relative composition of the  $\text{H}_2\text{SO}_4/\text{H}_2\text{O}_2$  solution impact the physical and chemical properties of titanium surfaces. Our aim is to achieve the capacity to precisely design titanium surfaces at the submicro and nanoscale to improve their biological response for different applications in medicine, such as orthopedic and dental implants.

#### Materials and Methods

##### Controlled Chemical Oxidation of cpTi Disks

Titanium disks 12 mm in diameter and 2 mm in thickness (Titanium Industries, Montréal, Québec, Canada) were mechanically polished to a mirror finish (PowerPro5000<sup>TM</sup>, Buehler, Lake Bluff, IL, USA) by using SiC grinding paper, then diamond paste, and finally a suspension of  $\text{SiO}_2$ . The polished disks were first cleaned with distilled water, then with toluene in an ultrasonic bath for respectively one hour and 15 min (Fisher Scientific, Fair Lawn, NJ, USA). Samples were finally dried in air.

To assess the effects of concentrated (95–97%, equivalent to 36N) sulfuric acid (J.T. Baker, Phillipsburg, NJ, USA),  $\text{H}_2\text{SO}_4^{\text{conc}}$ , and 30% aqueous hydrogen peroxide (Fisher Scientific),  $\text{H}_2\text{O}_2^{\text{aq}}$ , on titanium surface properties, the two singular reagents (henceforth indicated as solutions with respectively 0 and 100% of  $\text{H}_2\text{O}_2^{\text{aq}}$ ) and three solutions with different  $\text{H}_2\text{SO}_4^{\text{conc}}/\text{H}_2\text{O}_2^{\text{aq}}$ : volume ratios (i.e., 3:1, 1:1, 1:3,

henceforth indicated as Piranha solutions composed by 25, 50, and 75%  $\text{H}_2\text{O}_2^{\text{aq}}$ ) were used. Whereas the use of singular reagents did not require any special preparation, for the three  $\text{H}_2\text{SO}_4^{\text{conc}}/\text{H}_2\text{O}_2^{\text{aq}}$  solutions the acid was placed in a Pyrex glass container followed by the slow addition of appropriate quantities of hydrogen peroxide. Constant stirring was provided to guarantee a homogeneous mixing of the two components. The effect of temperature was also determined by carrying out the etching at four different temperatures, namely 5, 25, 50, and 80 °C. Freshly prepared  $\text{H}_2\text{SO}_4^{\text{conc}}/\text{H}_2\text{O}_2^{\text{aq}}$  solutions were cooled in ice to reduce their temperature to the desired value, due to the heat generated during mixing. Pyrex beakers with the reagents/solutions for etching at 5 °C were maintained in ice for the whole length of the treatment. Etching at 25, 50, and 80 °C was carried out by immersing the Pyrex glass container in an isothermal water bath placed on a stirring hot plate with an automatic feedback control (ECHOterm HS40, Torrey Pines Scientific, San Diego, CA, USA). After thermal equilibrium was reached, the titanium disks were placed in the glass container for 1 h. Longer intervals were also used to investigate the kinetics of topographical modifications. After etching was stopped, the recovered disks were rinsed with distilled water, washed further with ethanol, and subsequently dried in air, according to a previously established protocol.<sup>[15]</sup>

##### Reagents/Solutions Electrochemical Characterization

Reagents and solutions were characterized by their oxidative-reductive potential (ORP). ORP measures the redox potential through a potentiometric method that uses a reference electrode, an inert indicator electrode (Pt-Ag/AgCl electrode, Accumet, Fisher Scientific) and a potential reading meter (PH11 Series, Oakton, Vernon Hills, IL, USA). Prior to each measurement, calibration was carried out with a standard solution (ORP Standard, Orion Application Solution, Cole-Parmer, Vernon Hills, IL, USA), with a potential  $E_{\text{H}}$  referred to the normal hydrogen electrode (NHE) at 25 °C equal to +420 mV.

##### Structural Analysis

Surfaces of etched disks were examined by using a JEOL-JSM7400F field-emission scanning electron microscope (FE-SEM). Images were processed by analySIS<sup>®</sup> software (Soft Imaging System GmbH, Münster, Germany) to determine the evolution of the mean pit diameter with relative concentration and temperature. Variations in surface topography were also characterized by AFM in tapping mode using a JEOL JSPM-5200 instrument.

##### Fourier-Transform Infrared Spectroscopy (FT-IR)

IR was used to probe the modified oxide layer resulting from chemical treatment. A Nexus 870 FT-IR spectrometer equipped with a smart aperture grazing angle (SAGA) accessory (Thermo Nicolet, Madison, WI, USA) was used. Analysis of the thin oxide layer was performed in grazing angle mode at an angle of 80° with respect to the surface

normal, with a spectral resolution of  $4\text{ cm}^{-1}$  in the  $475\text{--}4000\text{ cm}^{-1}$  range. Spectroscopic information was collected from an  $8\text{ mm}$  diameter area. A gold substrate was used to collect a background spectrum. Spectra were finally fitted by PeakFit software (SPSS, Chicago, IL, USA) using Pearson VII functions as reported previously.<sup>[16,18]</sup>

*Wettability: Contact Angle Measurements*

Contact angles were obtained using the sessile drop method.<sup>[22]</sup> Images of drops ( $10\text{ mL}$  of  $18.2\text{ MW cm}^{-1}$  water) were recorded with a contact angle goniometer NRL-100 (Rame-Hart, Netcong, NJ, USA) after  $30\text{ s}$ .

*Results*

ORP measurements have been used so far in many environmental applications such as in situ monitoring of the chlorination/dechlorination process<sup>[23]</sup> and recognition of oxidants/reductants<sup>[24]</sup> in wastewater, as well as in the observation of the cycle chemistry in power plants.<sup>[25]</sup> The outcome of these measurements is the overall potential of all the reactive electrochemical couples in the solution. Here, we demonstrate that this technique can be applied to unequivocally characterize and identify chemical solutions by their oxidation–reduction potential.

Figure 1 shows the effects of chemical composition and temperature on ORP values (referred to the NHE). Our data show that the oxidative potential does not significantly depend on temperature (although temperature affects the redox potential of an electrochemical couple according to Nernst's equation<sup>[26]</sup>). In addition, all the solutions used for this study present an oxidative nature (positive ORP). Their oxidative power decreases with the percentage of  $\text{H}_2\text{O}_2^{\text{aq}}$  until  $680 \pm 40\text{ mV}$  at  $25\text{ }^\circ\text{C}$  in the case of pure  $30\%$  aqueous hydrogen peroxide. These results can be correlated to a previous study<sup>[27]</sup> which illustrates that when aqueous  $\text{H}_2\text{O}_2$  is brought in contact with  $\text{H}_2\text{SO}_4$ , two new oxidation agents, namely  $\text{HSO}_5^-$  and  $\text{H}_3\text{O}_2^+$ , are created in solution. The presence of such new oxidative agents could explain the higher positive ORP value of  $\text{H}_2\text{SO}_4^{\text{conc}}/\text{H}_2\text{O}_2^{\text{aq}}$  mixtures compared to that of  $\text{H}_2\text{O}_2^{\text{aq}}$ . In the case of concentrated sulfuric acid, this technique did not yield to meaningful readings, probably due to the fact that  $\text{H}_2\text{SO}_4^{\text{conc}}$  does not present sufficient reactive redox couples due to the small presence of water.

SEM micrographs of titanium disks exposed to different etching reagents were used to classify the resulting surfaces according to their topographical features into four categories: (A) no texture; (B) nanotexture; (C) nano- and submicro texture; and (D) not applicable (i.e., without distinctive and repro-

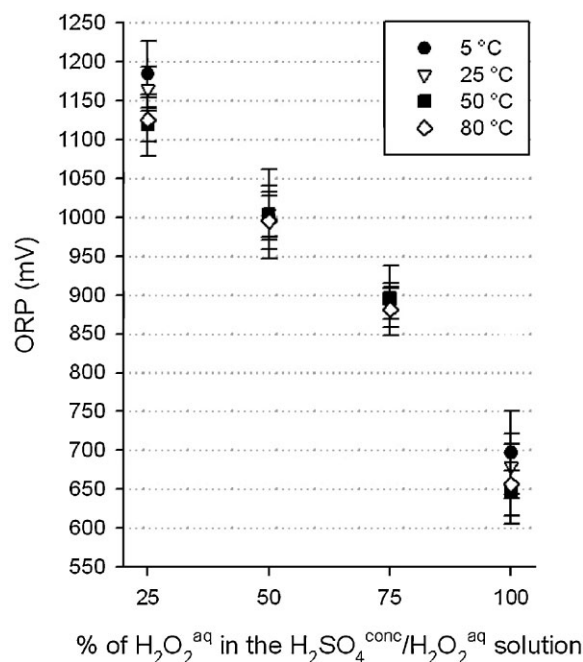


Fig. 1. ORP of  $\text{H}_2\text{SO}_4^{\text{conc}}/\text{H}_2\text{O}_2^{\text{aq}}$  solutions referred to the NHE.

ducible features) (Fig. 2). AFM images of patterned surfaces are shown in Figure 3. Samples belonging to category A present smooth surfaces with no distinctive topographical features aside from polishing grooves. Disks classified in category B reveal the characteristic nanotexture<sup>[15,16]</sup> resulting from treatment of titanium with the  $\text{H}_2\text{SO}_4^{\text{conc}}/\text{H}_2\text{O}_2^{\text{aq}}$  solution. Samples from group C show a submicrotexture with a

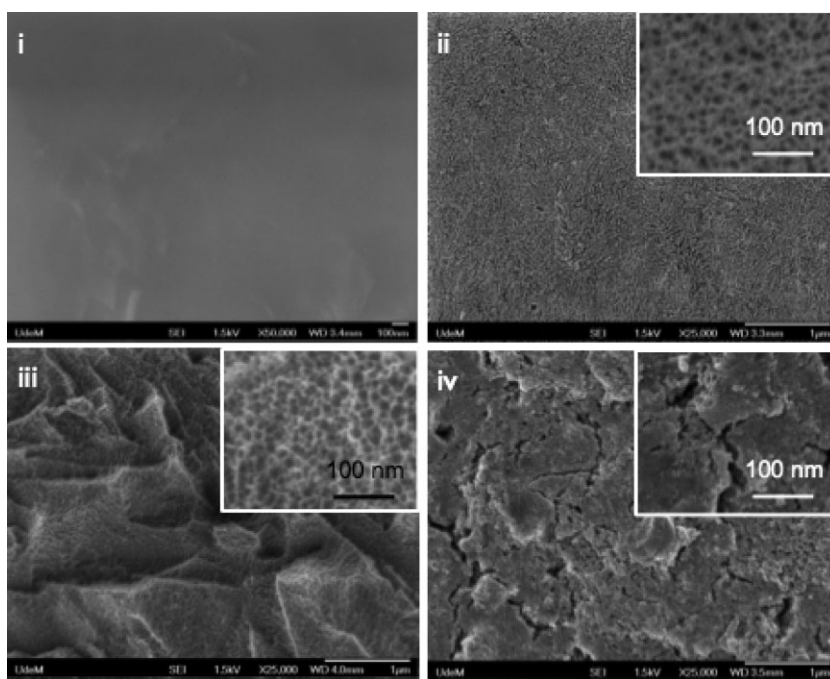


Fig. 2. SEM images of (i) smooth titanium surfaces (category A), (ii) nanotextured titanium surfaces (category B), (iii) titanium surfaces presenting a submicrotexture with a superimposed nanotexture (category C), and (iv) titanium surfaces without distinctive patterns (category D).

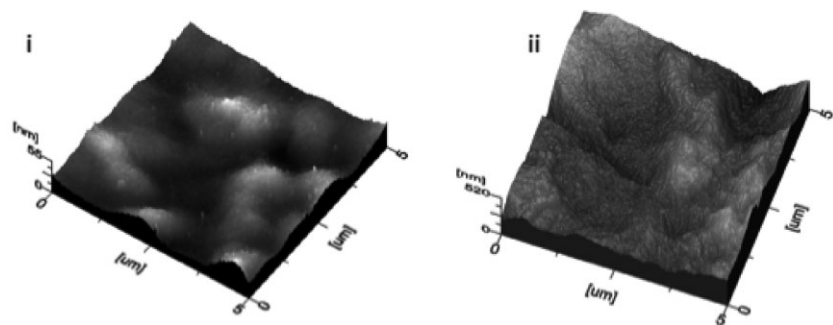


Fig. 3. AFM images of (i) nanotextured and (ii) submicro and nanotextured titanium surfaces.

required to create the nanotexture. To determine the precise  $H_2SO_4^{conc}:H_2O_2^{aq}$  ratio at which nanotexture starts to form at room temperature, we systematically varied the composition by gradually increasing the amount of hydrogen peroxide in solution. When the volumetric percentage of  $H_2O_2^{aq}$  reached 30%, isolated circular nanopits appeared randomly distributed on the smooth titanium surface after 1 h of treatment [Fig. 4(i)]. Surfaces presenting a more homogeneous nanoporous network were achieved by augmenting the presence of hydrogen peroxide to 35% [Fig. 4(ii)].

superimposed nanoporous structure. AFM linear scans revealed that the depth of the submicrometric features is in the 200–300 nm range. Samples within category D present surfaces with no distinctive micro- or nanometric patterns. Table 1 displays this classification as a function of the nature and temperature of the etchants. Our data show that concentrated  $H_2SO_4$  is not able to create any texture in the range of temperature considered, although it was reported<sup>[28]</sup> that a more diluted sulfuric acid (48%, equivalent to 9M) at 60 °C can create a microporous structure on titanium. In addition, our results show that at 5 °C none of the solutions has an effect on topography, not even the one (i.e., 50% v/v  $H_2SO_4^{conc}/H_2O_2^{aq}$ ) which proved already to be able to nanopattern titanium and Ti6Al4V at room temperature (~25 °C).<sup>[15–18]</sup>

At 50 and 80 °C, surfaces treated with  $H_2SO_4^{conc}/H_2O_2^{aq}$  mixtures exhibit a rough submicrometric structure with a superimposed nanotopography. Etching with hydrogen peroxide alone in this range of temperature produced a rough surface layer with several visible cracks. The mean nanopit diameter was systematically determined by detailed image analysis. The equivalent circle diameter (ECD) was determined with analySIS<sup>®</sup> software for the nanotextured disks. The majority of surfaces exhibits a mean pit diameter of  $20 \pm 6$  nm, in agreement with our previous results.<sup>[16,18]</sup> However, solutions composed by 75% in volume of hydrogen peroxide yielded to higher mean values and statistical dispersion, namely  $26 \pm 9$  and  $24 \pm 9$  nm at 50 and 80 °C, respectively.

At 25 °C, all the reagents yielded nanoporous structures, except for the 3:1  $H_2SO_4^{conc}/H_2O_2^{aq}$  solution which did not produce any micro- or nanometric surface modification. These findings suggest that (i)  $H_2O_2^{aq}$  alone can create a nanoporous surface at room temperature and that (ii) there is a minimum concentration of  $H_2O_2^{aq}$  (between 25 and 50% in volume)

In a previous report,<sup>[18]</sup> we demonstrated a close relation between the integrated area of the IR peaks related to the Ti–O bonds and the thickness of the oxide layer. Figure 5 displays the quantitative evolution of the integrated area of the absorption band in the 400–1000  $cm^{-1}$  range, which is thought to be related to  $TiO_2$  thickness. A more detailed analysis of the quantitative relation between the growth of intensity of the IR

Table 1. Topographical modifications resulting from varying the parameters of chemical oxidation with  $H_2SO_4^{conc}/H_2O_2^{aq}$  mixtures

Solution Temp.	$H_2SO_4^{conc}$	75% $H_2SO_4^{conc}$ 25% $H_2O_2^{aq}$	50% $H_2SO_4^{conc}$ 50% $H_2O_2^{aq}$	25% $H_2SO_4^{conc}$ 75% $H_2O_2^{aq}$	$H_2O_2^{aq}$	
	5 °C	⊗	⊗	⊗	⊗	⊗
25 °C	⊗	⊗	✓	✓	✓	✓ Nano texture
50 °C	⊗	✓	✓	✓	?	✓ Nano and SubMicro texture
80 °C	⊗	✓	✓	✓	?	? Not Applicable

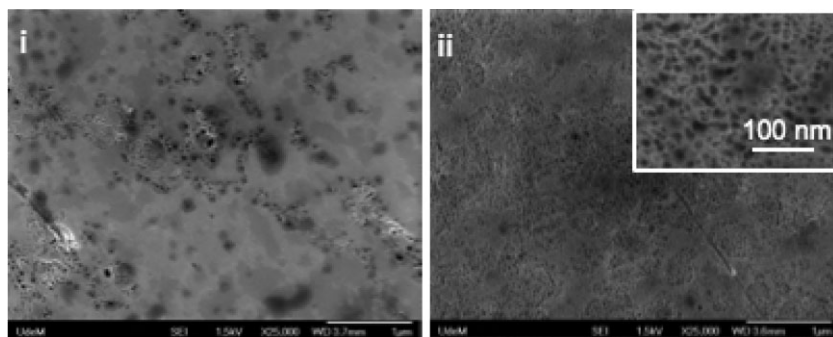


Fig. 4. SEM images of titanium surfaces resulting from 1 h of treatment at 25 °C with (i) 70% $H_2SO_4^{conc}$  / 30% $H_2O_2^{aq}$  and (ii) 65% $H_2SO_4^{conc}$  / 35% $H_2O_2^{aq}$ .

band and the oxide thickness as estimated by ellipsometry has been described elsewhere.<sup>[29]</sup> Compared to polished controls (total integral area  $2.0 \pm 0.5$  a.u.), only nanotextured surfaces show an increase in the absorption band's integral area/intensity (e.g., treatments which did not result in topographical modifications, such as the ones with  $H_2SO_4^{conc}$  and 75% $H_2SO_4^{conc}$  / 25% $H_2O_2^{aq}$  at 25 °C, did not present any significant variation in the Ti–O band's intensity), corresponding to an estimated  $TiO_2$  layer in the 40–60 nm range. Spectroscopic data collected in the case of etching with  $H_2O_2^{aq}$  at 50 and 80 °C indicate the presence of a much thicker layer of amorphous  $TiO_2$ .

Due to their apparent simplicity and straightforwardness, contact angle measurements have been extensively used to determine the wettability and free energy of surfaces, especially in biomedical related research, since these parameters are considered to affect cell attachment and spreading.<sup>[30–32]</sup> However, data resulting from this technique should be interpreted with care. Several reports have highlighted its limitations and the possible mistakes which can occur during contact angle data analysis.<sup>[22,33,34]</sup> Surface roughness, chemical inhomogeneity, and the presence of adsorbates (such as

hydrocarbon contaminants) are all factors that should be cautiously considered to avoid misleading data interpretation. Chemical homogeneity of controls and treated samples was validated by our previous X-ray photoelectron spectroscopy (XPS) results.<sup>[16,18]</sup> Nevertheless, our goal is to obtain qualitative information on overall surface wettability by measuring the apparent contact angle, without distinction whether it is related to roughness, porosity, free energy or the presence of contaminants. In Figure 6, we reported the measured values of contact angles without corrections. The majority of surfaces is more hydrophilic than smooth

controls. Only samples treated with 25% $H_2SO_4^{conc}$  / 75% $H_2O_2^{aq}$  and  $H_2O_2^{aq}$  at 5 °C show contact angles similar to those measured on polished surfaces.

### Discussions

By comparing Figure 1 and Table 1, we infer that the oxidative potential of  $H_2SO_4^{conc}$  /  $H_2O_2^{aq}$  solutions does not determine the formation of a superficial nanotexture on titanium. In fact, although the 75% $H_2SO_4^{conc}$  / 25% $H_2O_2^{aq}$  solution presents the highest ORP values, at 25 °C this mixture does not create any surface pattern. Considering that (i) its ORP at 50 and 80 °C does not vary dramatically from that measured at room temperature and (ii) at these temperatures micro- and nanotextures are present, we can deduce that this electrochemical property does not predict the effects of the solution on micro- and nanotopography. From these results, we infer that nanotexturing has a thermodynamic/kinetic barrier which has to be overcome for the process to be initiated. It is observed that  $H_2SO_4^{conc}$  or solutions with less than 30% of  $H_2O_2^{aq}$  are not able to surmount it and affect consequently the topography, thus indicating that there is a

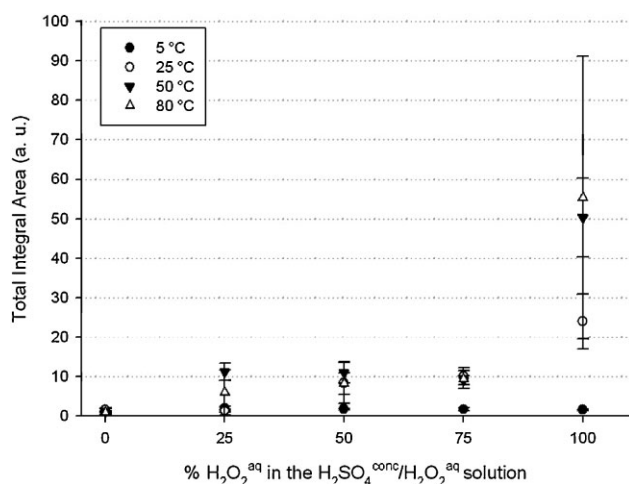


Fig. 5. Graph showing integrated Ti–O absorbance (FT-IR) as a function of percentage of  $H_2O_2^{aq}$  and temperature of the etching solution.

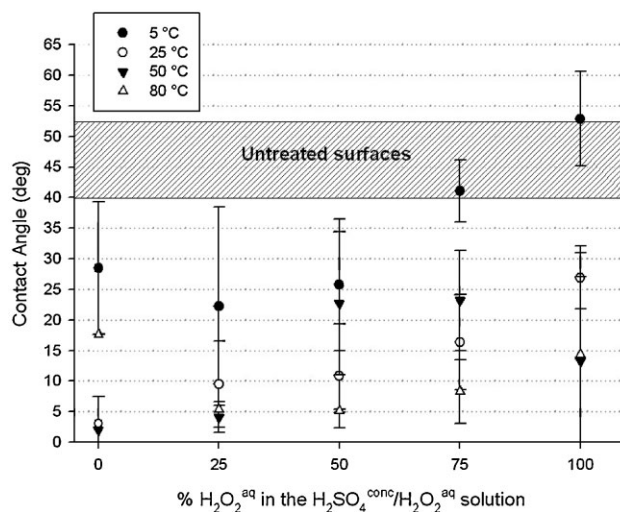


Fig. 6. Graph showing contact angle values as a function of percentage of  $H_2O_2^{aq}$  and temperature of the etching solution.

minimum concentration of hydrogen peroxide required to create micro- or nanopatterns on titanium. While  $\text{H}_2\text{SO}_4^{\text{conc}}$  did not produce any appreciable topographical modification for all the conditions examined in this study, the  $75\%\text{H}_2\text{SO}_4^{\text{conc}}/25\%\text{H}_2\text{O}_2^{\text{aq}}$  solution was able to micro- and nanotexture titanium at higher temperatures. In other words, supplementary energy has to be added to this system to overcome the energy barrier. To verify whether this solution does not have the thermodynamic capacity to create a nanotexture at  $25^\circ\text{C}$ , we decided to extend the chemical treatment to 18 h. This mixture was observed to create a nanotopography at room temperature after this longer period. This demonstrates that surface nanotexturing depends on time (as previously demonstrated in the case of the Ti6Al4V alloy<sup>[17,18]</sup>) as well as on temperature and relative composition, as long as the etchant possesses reactive species in solution which may come from either the decomposition of  $\text{H}_2\text{O}_2^{\text{aq}}$  or from the reaction products in  $\text{H}_2\text{SO}_4^{\text{conc}}/\text{H}_2\text{O}_2^{\text{aq}}$  mixtures. Etching with the sole  $\text{H}_2\text{SO}_4^{\text{conc}}$  for a longer interval (18 h) at room temperature did not significantly modify the titanium's nanotopography. However, occasional isolated micrometric areas showed a microporosity similar to the one described by Ban *et al.*<sup>[28]</sup> (Fig. 7). We hypothesize that even a minimal presence of water in  $\text{H}_2\text{SO}_4^{\text{conc}}$  (3–5% plus possible contribution from the atmosphere) can participate in creating reactive couples in solution which can slowly micro-pattern titanium surfaces. The use of different mixtures consisting of acid/bases and oxidants of variable strengths may allow to overcome at room temperature the energy required and generate novel nanometric patterns on implantable metals. In fact, mixtures composed by ammonium hydroxide ( $\text{NH}_4\text{OH}$ ) and  $\text{H}_2\text{O}_2^{\text{aq}}$  created, at  $25^\circ\text{C}$ , a reproducible network of pits in the 50–100 nm range on relevant implantable metals (i.e., cpTi, Ti6Al4V, and Tantalum).<sup>[21]</sup>

Image analysis indicates that the average diameter of nanopits does not vary with etching conditions. Nevertheless, some of the solutions used for this study, yielded pores with slightly larger diameters, presumably resulting from the

joining of individual pits or from cracks on the oxide layer. These results indicate that the pit diameter strongly depends on the identity of the chemical solution and is not a function of the etching parameters. To generate different nanoporous patterns with significantly different morphological and chemical properties, it is thus necessary to vary the specific nature of the etchants.<sup>[21]</sup>

To understand the relative effect on nanotexturing arising from concentrated sulfuric acid and aqueous hydrogen peroxide, we replaced  $\text{H}_2\text{SO}_4^{\text{conc}}$  with ultrapure water ( $18.2\text{MW cm}^{-1}$ ) in the different mixtures used. Similarly to the previous results obtained with sulfuric acid in solution, at room temperature, nanoporosity was detected by SEM on samples treated for one hour with solutions having  $\text{H}_2\text{O}_2^{\text{aq}}$  in concentrations higher than 25% (Fig. 8).

These findings indicate that: (i) for each of the tested solutions, the presence of  $\text{H}_2\text{O}_2^{\text{aq}}$  (more generally of an oxidative agent<sup>[21]</sup>) is a prerequisite to nanotexture titanium; (ii) for each nanotexturing solution at a fixed temperature, there is a minimum time required to initiate the nanotexturing process; (iii) while temperature has no significant effect on oxidative potential, it can be advantageously exploited to accelerate creation of topography; (iv) on the other hand, concentration of  $\text{H}_2\text{O}_2^{\text{aq}}$  affects the oxidative potential and the speed at which texture forms; and (v) the presence of sulfuric acid is not fundamental to create nanotexture.<sup>[21]</sup> However, its presence creates a more uniform surface with nanometric pits that are better defined (Fig. 9).

Etching with the  $75\%\text{H}_2\text{SO}_4^{\text{conc}}/25\%\text{H}_2\text{O}_2^{\text{aq}}$  solution for 18 h yielded another interesting result. Parallel grooves appeared within grains of nanotextured titanium surfaces (Fig. 10). These micrometric furrows are likely related to a preferential etching process in areas where the local metallurgic and/or crystallographic properties may cause variations in the corrosion potential, as it was reported in the case of dislocation pile-ups.<sup>[35,36]</sup> Qualitative image analysis suggested that the number of grains affected by this phenomenon dramatically

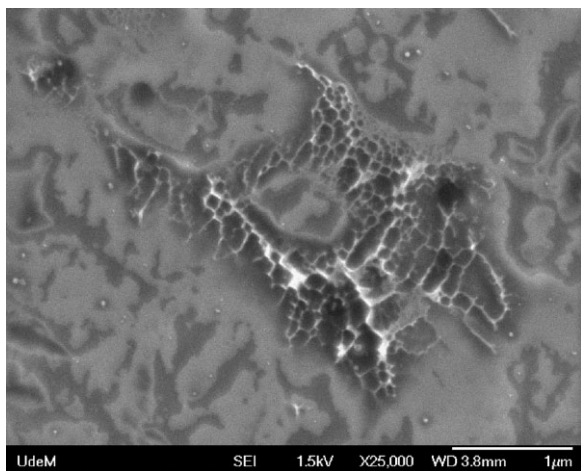


Fig. 7. SEM image of titanium surface treated with concentrated  $\text{H}_2\text{SO}_4^{\text{conc}}$  for 18 h at  $25^\circ\text{C}$ .

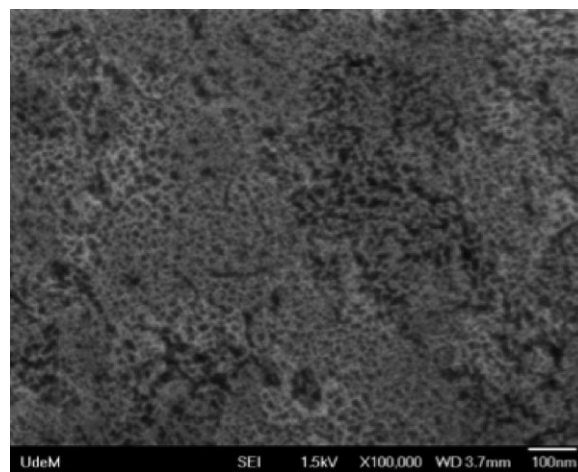


Fig. 8. SEM image of nanotexture resulting from one hour of treatment on titanium using diluted 30% aqueous hydrogen peroxide ( $50\% \text{H}_2\text{O}_2^{\text{aq}} / 50\% \text{ultrapure water}$  at  $25^\circ\text{C}$ ).

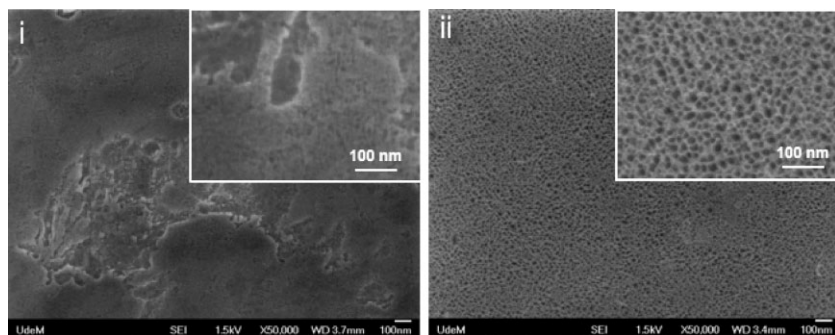


Fig. 9. SEM images of titanium surfaces resulting from one hour of (i) 50%  $H_2O_2^{aq}$  /50% ultrapurewater and (ii) 50%  $H_2SO_4^{conc}$  /50%  $H_2O_2^{aq}$  treatment at 25 °C.

decreases by increasing either etching time (in our case we extended the treatment to 36 h) or the concentration of  $H_2O_2^{aq}$  (25%  $H_2SO_4^{conc}$  /75%  $H_2O_2^{aq}$ ), giving rise to the previously described submicrotexture. This implies that the creation of parallel submicrometric grooves, along with cavities in correspondence to grain boundaries, is an intermediate step which occurs before the formation of the submicrotexture. Unlike the case of Ti6Al4V, where the submicrotexture resulted from a differential etching of the two crystallographic phases of the alloy,<sup>[18]</sup> the present submicrometric topographical features are believed to derive from a directional and non-uniform etching along crystalline planes/directions of the metallic grains which are more susceptible to attack.

IR data (Fig. 3) reveal that there is no correspondence between the ORP and the increase in the oxide thickness estimated by FT-IR. This demonstrates that a higher ORP value does not produce a more efficient oxidation of titanium with the consequent growth of the oxide layer. On the contrary, the solution with the lowest ORP, namely  $H_2O_2^{aq}$ , created a very thick oxide (about 20–50 times thicker than control). Instead, it appears that an increase in the  $TiO_2$  thickness depends on the presence of superficial nanoporosity which permits the solution to reach and oxidize the underlying metal throughout the nanopitted oxide, consistent with our previous model.<sup>[18]</sup>

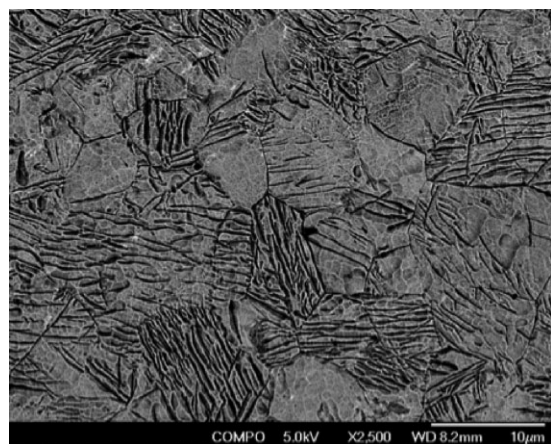


Fig. 10. SEM image of the submicrometric grooves resulting from directional etching on titanium grains.

At 50 and 80 °C,  $H_2O_2^{aq}$  lost its ability to create a regular topography, essentially yielding rough but unstructured amorphous  $TiO_2$  superficial layers. This observation is not consistent with previous reports indicating that aqueous hydrogen peroxide at 80 °C can create nano/submicrometric surface structures on titanium.<sup>[37,38]</sup> We attribute this discrepancy to a difference between the experimental parameters used (concentration and pressure). We believe that the conditions we have used may generate an intense and uncontrolled oxidation reaction. In this context, preliminary studies

revealed that conditions which lead to the build up of pressure during etching with  $H_2O_2^{aq}$  (sealed vs. open reaction vessels) influence the outcome of the chemical treatment (data not shown).

All the new generated surfaces exhibited enhanced hydrophilicity compared to controls. While this result was expected on micro- and nanotextured surfaces<sup>[17,39]</sup> due to their physical (e.g., roughness and porosity) and chemical (e.g., minor presence of contaminants<sup>[15]</sup>) characteristics, the low contact angles resulting from treatment conditions that yield smooth surfaces were unexpected. We believe that this derives from the removal of possible adsorbates which are typically present on untreated samples.  $H_2SO_4^{conc}$  /  $H_2O_2^{aq}$  solutions can be thus selected to clean efficiently surfaces, even at low temperature (5 °C), without modifying their topography. However, there is a concentration of  $H_2O_2^{aq}$  (between 50 and 75%) above which the process appears to be inefficient. Consequently, solutions richer in  $H_2SO_4^{conc}$  provide a more efficient cleaning of titanium surfaces at lower temperatures.

Our findings suggest that the first effect of oxidative treatment with  $H_2SO_4^{conc}$  /  $H_2O_2^{aq}$  is the removal of superficial contaminants leading to hydrophilicity. After a suitable exposure time, the nanotexture starts to develop on the native  $TiO_2$  layer from isolated and randomly distributed nanopits to a complex three-dimensional nanoporous network which additionally contributes to wettability. We believe that the nanometric foci where the first pits are nucleated correspond to sites of electrochemical discontinuity. Such sites, including metallurgical defects, presence of heterogeneous inclusions, and local differences in oxide thickness, would have a higher susceptibility to etching. As the sponge-like network of nanopits is created, the etching solution penetrates throughout the protective oxide layer to reach the underlying metal. Concomitant dynamic processes take place: a directional attack of the metallic grains (preceded by the selective corrosion of weaker areas such as grain boundaries and dislocation pile-ups for instance), a selective removal of the outer oxide layer (which yields the nanometric pits) and an oxidation of the metal. The final result is the creation of a submicron topography covered by a thicker nanoporous  $TiO_2$ .

In a study using a titanium alloy and where sulfuric acid was used for anodization,<sup>[40]</sup> it was demonstrated that selective etching of grains and nanoscale surface modifications do not affect the mechanical properties of the material. The authors actually showed that the treatment improved fatigue strength. Therefore, accordingly, we believe that fatigue strength should not be compromised by our chemical oxidation process, thus this approach is applicable to implants that are subject to mechanical stress and fatigue cycles.

### Conclusion

Our work demonstrates that by varying etching parameters such as solution composition, temperature, and exposure time, it is possible to modify the topography, oxide thickness and wettability of commercially pure titanium. Thus chemical oxidation with  $\text{H}_2\text{SO}_4^{\text{conc}}/\text{H}_2\text{O}_2^{\text{aq}}$  solutions is an efficient tool to achieve various physical and chemical configurations on this medically-relevant metal. Hydrophilic smooth surfaces (e.g., to study the effect of wettability/free energy on cell behavior), bioactive nanotextures as well as submicrotextures with a superimposed nanopattern (for in vitro and in vivo studies and for applications where more than one level of topography is required), parallel submicrometric grooves (which may provide a more suitable substrate for the mechanical anchorage of bioactive coatings) can all be designed.

Received: May 5, 2009

Final Version: July 14, 2009

- [1] D. G. Poitout, K.-G. Thorngren, R. Kotz, *Biomechanics and Biomaterials in Orthopedics* Springer London **2004**.
- [2] J. Y. Wong, J. D. Bronzino, *Biomaterials* CRC Press **2007**.
- [3] J. Black, *Biological Performance of Materials: Fundamentals of Biocompatibility* CRC Press **2006**.
- [4] P. Wooley, E. Schwarz, *Gene Ther.* **2004**, *11*, 402.
- [5] D. Castner, B. Ratner, *Surf. Sci.* **2002**, *500*, 28.
- [6] M. J. Dalby, N. Gadegaard, R. Tare, A. Andar, M. O. Riehle, P. Herzyk, C. D. W. Wilkison, R. O. C. Oreffo, *Nat. Mater.* **2007**, *6*, 997.
- [7] M. M. Stevens, J. H. George, *Science* **2005**, *310*, 1135.
- [8] E. K. Yim, K. W. Leong, *Nanomedicine* **2005**, *1*, 10.
- [9] K. Anselme, *Biomaterials* **2000**, *21*, 667.
- [10] J. B. Brunski, D. A. Puleo, A. Nanci, *Int. J. Oral. Maxillofac. Implants* **2000**, *15*, 15.
- [11] B. Kasemo, J. Gold, *Adv. Dent. Res.* **1999**, *13*, 8.
- [12] A. Bagno, C. D. Bello, *J. Mater. Sci. : Mater. Med.* **2004**, *15*, 935.
- [13] X. Liu, P. K. Chu, C. Ding, *Mater. Sci. Eng., R* **2004**, *47*, 49.
- [14] F. Variola, F. Vetrone, L. Richert, P. Jedrzejowski, S. Z. J. H. Yi, S. Clair, A. Sarkissian, D. F. Perepichka, J. D. Wuest, F. Rosei, A. Nanci, *Small* **2008**, *5*, 996.
- [15] A. Nanci, J. D. Wuest, L. Peru, P. Brunet, V. Sharma, S. F. Zalzal, M. D. McKee, *J. Biomed. Mater. Res.* **1998**, *40*, 324.
- [16] J.-H. Yi, C. Bernard, F. Variola, S. F. Zalzal, J. D. Wuest, F. Rosei, A. Nanci, *Surf. Sci.* **2006**, *600*, 4613.
- [17] L. Richert, F. Vetrone, J.-H. Yi, S. F. Zalzal, J. D. Wuest, F. Rosei, A. Nanci, *Adv. Mater.* **2008**, *20*, 1488.
- [18] F. Variola, J.-H. Yi, L. Richert, J. D. Wuest, F. Rosei, A. Nanci, *Biomaterials* **2008**, *29*, 1285.
- [19] P. T. d., Oliveira, S. F. Zalzal, M. M. Beloti, A. L. Rosa, A. Nanci, *J. Biomed. Mater. Res., Part A* **2007**, *80*, 554.
- [20] P. T. d., Oliveira, S. F. Zalzal, K. Irie, A. Nanci, *J. Histochem. Cytochem.* **2003**, *51*, 633.
- [21] F. Vetrone, F. Variola, P. T. d., Oliveira, S. F. Zalzal, J.-H. Yi, J. Sam, K. F. Bombonato-Prado, A. Sarkissian, D. F. Perepichka, J. D. Wuest, F. Rosei, A. Nanci, *Nanoletters* **2009**, *9*, 659.
- [22] A. Marmur, *Soft Matter* **2006**, *2*, 12.
- [23] J. A. Bergendahl, L. Stevens, *Environ. Chem.* **2005**, *24*, 214.
- [24] J.-H. Lee, A. Jang, P. R. Bhadri, R. R. Myers, W. Timmons, F. R. B. Jr., P. L. Bishop, I. Papautsky, *Sens. Actuators, B* **2006**, *115*, 220.
- [25] L. Cave, N. Hartog, T. Al, B. Parker, K. U. Mayer, S. Cogswell, *Ground Water Monit. Rem.* **2007**, *27*, 77.
- [26] C. H. Hamann, A. Hamnett, W. Vielstich, *Electrochemistry*, Wiley **2007**.
- [27] A. N. Ermakov, I. K. Larin, Y. N. Kozlov, A. P. Purmal, *Russ. J. Phys. Chem.* **2006**, *80*, 1895.
- [28] S. Ban, Y. Iwaya, H. Kono, H. Sato, *Dent. Mater.* **2006**, *22*, 1115.
- [29] F. Variola, A. Nanci, F. Rosei, *Appl. Spectrosc.* **2009**, *63*, 1187.
- [30] J. Wei, M. Yoshinari, S. Takemoto, M. Hattori, E. Kawada, B. Liu, Y. Oda, *J. Biomed. Mater. Res., Part B: Appl. Biomater.* **2007**, *81*, 66.
- [31] S. A. Redey, S. Razzouk, C. Rey, D. Bernache-Assollant, G. Leroy, M. Nardin, G. Cournot, *J. Biomed. Mater. Res.* **1999**, *45*, 140.
- [32] K. Webb, V. Hlady, P. A. Tresco, *J. Biomed. Mater. Res.* **1998**, *41*, 422.
- [33] S. Brandon, N. Haimovich, E. Yeger, A. Marmur, *J. Colloid Interface Sci.* **2003**, *263*, 237.
- [34] T. S. Meiron, A. Marmur, I. S. Saguy, *J. Colloid Interface Sci.* **2004**, *274*, 637.
- [35] E. M. Gutman, *Mechanochemistry of Solid Surfaces*, World Scientific Publishing Co. Ltd., **1994**.
- [36] F. A. Martin, C. Bataillon, J. Cousty, *Corros. Sci.* **2008**, *50*, 84.
- [37] J.-M. Wu, S. Hayakawa, K. Tsuru, A. Osaka, *Scr. Mater.* **2002**, *46*, 101.
- [38] A. S. Zuruzi, N. C. MacDonald, *Adv. Funct. Mater.* **2005**, *15*, 396.
- [39] S. Clair, F. Variola, M. Kondratenko, P. Jedrzejowski, A. Nanci, F. Rosei, D. F. Perepichka, *J. Chem. Phys.* **2008**, *128*, 144705.
- [40] C. Leinenbach, D. Eifler, *Biomaterials* **2006**, *277*, 1200.